

FREQUENCY DEPENDENT ATTENUATION ANALYSIS OF GROUND-PENETRATING RADAR DATA

John H. Bradford, CGISS, Boise State University, Boise, ID

Abstract

I investigate the frequency dependence of attenuation and problems with measuring the intrinsic attenuation in reflection data. It is well established that in many materials attenuation is approximately linear with frequency over the bandwidth of the GPR signal, with a slope characterized by a constant Q^* parameter. I show the relationship of Q^* to the parameters describing Cole-Cole relaxation and that when the dominant GPR frequency is well above or below the primary relaxation frequency, Q^* is a simple function of the ratio of real to imaginary parts of the dielectric permittivity. However, near the relaxation frequency, a more complicated function is required to describe the slope of the attenuation curve. For some materials relaxation occurs in the range from 10 - 200 MHz which is in the primary range that GPR operates for many applications. Adding to this complication is the often overlooked problem of frequency dependent reflection which can be significant in typical field conditions. Despite these complications, frequency dependent attenuation analysis of reflection data can provide valuable subsurface information. In two field examples I demonstrate that frequency-dependent attenuation analysis can locate anomalies associated with non-aqueous phase liquid contaminants.

Introduction

Electromagnetic waves propagating through the subsurface are subject to frequency dependent attenuation which depends on the effective conductivity. The effective conductivity is a function of the real component of the electric conductivity and the complex component of the dielectric permittivity. Turner and Siggins (1994) showed that a frequency independent quality factor (Q^*) can approximate the frequency dependent component of GPR attenuation in many cases.

To extract Q^* from field data, it is necessary to analyze spectral variation of the GPR signal through time, which is the basis of time-frequency (t-f) analysis (Bradford, 1999; Bradford and Wu, 1997; Chakraborty and Okaya, 1995; Irving and Knight, 2003; Li and Ulrych, 1996; Morlet et al., 1982a, b; Tobbock et al., 1996). With an accurate measure of the t-f distribution, a number of methods are available to measure the frequency dependent component of attenuation including spectral ratios (e.g. Bradford, 1999) and the frequency shift method (Liu et al., 1998).

Material property characterization using attenuation analysis is relatively common in crosswell studies (Chang et al., 2002; Day-Lewis et al., 2002; Day-Lewis et al., 2003; Goldstein et al., 2003; Grandjean et al., 2000; Lane et al., 2000; Peterson, 2001; Zhou and Liu, 2001). However, development and evaluation of surface-based, reflection attenuation analysis remains limited. A few authors have addressed the problem for GPR. For example Turner (1994) and Irving and Knight (2003) describe methods for estimating Q^* and applying a deconvolution filter to GPR data to compensate for frequency dependent losses. Other studies suggest the potential for using a measure of reflection attenuation for direct material property characterization (Bradford, 1999; Cai and McMechan, 1999; Liu and Quan, 1997) but further work is needed.

Here, I first derive the relationship between Q^* and the Cole-Cole relaxation parameters (Cole and Cole, 1941). Next, I demonstrate that frequency dependent reflection can significantly distort the spectrum

and mask the intrinsic Q^* measurement. Finally, I show that despite a number of recognized complications, frequency dependent attenuation analysis can be a strong indicator of variation in bulk subsurface dispersion properties. At two field sites I demonstrate significant anomalies associated with both dense and light non-aqueous phase liquid contaminants.

Methodology

Linearizing the Attenuation Coefficient

For plane waves, the monochromatic propagating electric field is given by

$$\tilde{E}(\mathbf{r}, t) = \tilde{E}_0 e^{i(\tilde{k}\mathbf{r} - \omega t)} \quad (1)$$

where the complex wavenumber is given by

$$\tilde{k} = \beta + i\alpha \quad (2)$$

and

$$\alpha = \omega \left[\frac{\epsilon\mu}{2} \left(\sqrt{1 + \left(\frac{\sigma}{\epsilon\omega} \right)^2} - 1 \right) \right]^{\frac{1}{2}} \quad (3)$$

$$\beta = \omega \left[\frac{\epsilon\mu}{2} \left(\sqrt{1 + \left(\frac{\sigma}{\epsilon\omega} \right)^2} + 1 \right) \right]^{\frac{1}{2}} \quad (4)$$

where ω is the angular frequency, ϵ is the dielectric permittivity, σ is the electric conductivity, and μ is the magnetic permeability. By Equation 1, the complex part of the wavenumber gives the attenuation and the real part of the wavenumber gives the phase velocity by the relationship $v_{ph} = \omega/\beta$.

In general ϵ , μ , and σ are also complex quantities and Equations 3 and 4 are given in terms of real effective permittivity, ϵ_e , and real effective conductivity, σ_e , where

$$\epsilon_e = \epsilon' - \sigma''/\omega \quad (5)$$

$$\sigma_e = \sigma' + \epsilon''\omega \quad (6)$$

For radar it is typically taken that σ' is the DC conductivity ($\sigma' = \sigma_{dc}$) and $\sigma'' = 0$. In the low loss approximation $\sigma_e \ll \epsilon_e \omega$, and this is the condition under which GPR operates effectively. Using this approximation and the binomial expansion, Equation 3 reduces to (Griffiths, 1989)

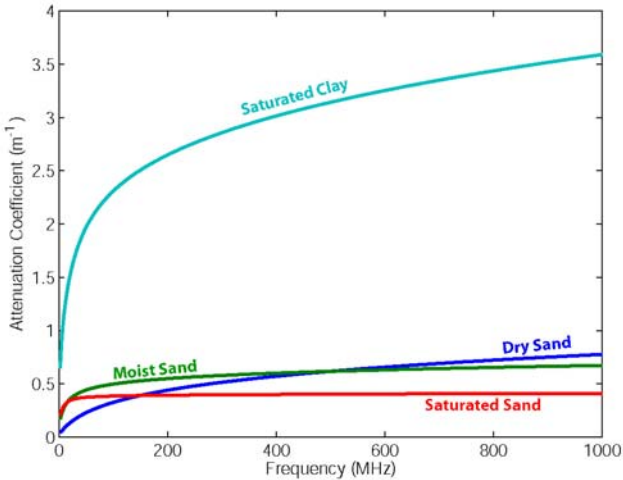
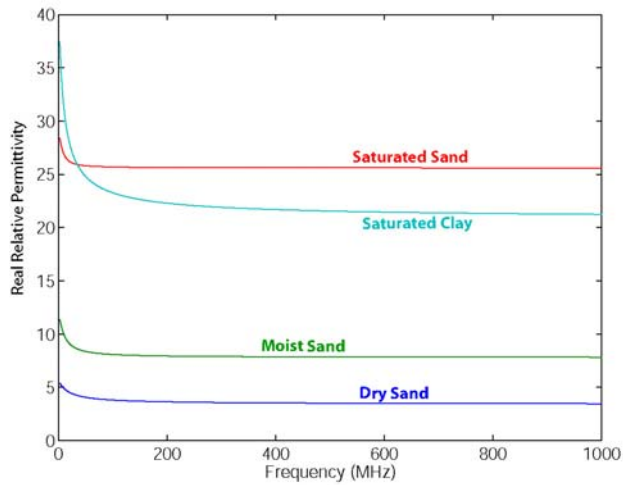


Figure 1: Frequency dependence of the real part of the dielectric permittivity and the attenuation coefficient (imaginary part of the wavenumber). The attenuation is dominated by the imaginary part of the dielectric permittivity.

heterogeneous materials. Similarly, Olhoeft (1974) demonstrated that for many materials the magnetic permeability is described by Cole-Cole relaxation. Figure 1 shows real permittivity and attenuation coefficient curves for dry sand, moist sand, water saturated sand, and clay with Cole-Cole parameters given in Table 1. Note that a GPR operating at 100 MHz would undergo significant dispersion in all of these

If the permittivity is real and independent of frequency, the attenuation is also frequency independent. The same approximation and assumptions shows that velocity is frequency independent and therefore there is no dispersion. However, the dielectric permittivity of earth materials is complex and from Equations 6 and 7 the attenuation is frequency dependent

$$\alpha = \frac{\sigma_e}{2} \sqrt{\frac{\mu}{\epsilon_e}} \quad (7)$$

$$\alpha \approx [\sigma_{dc} + \epsilon''(\omega) \omega] \frac{1}{2} \sqrt{\frac{\mu_0}{\epsilon'(\omega)}} \quad (8)$$

The frequency dependence of many earth materials is described with a Cole-Cole relaxation mechanism which gives the complex dielectric permittivity as (Cole and Cole, 1941)

$$\epsilon' - i\epsilon'' = \epsilon_\infty + \frac{\epsilon_{dc} - \epsilon_\infty}{1 + (i\omega\tau)^\gamma} \quad (9)$$

where τ is the primary relaxation time and the fit parameter γ allows for the superposition of multiple relaxation mechanisms that may be observed in

Table 1: Cole-Cole parameter for dielectric permittivity and magnetic permeability. The values for the three sands are given by Powers and Olhoeft (1995), and the values for clay are given by Olhoeft and Capron (1994).

Layer	K_0	K_∞	τ_ϵ (ns)	γ_ϵ	M_0	M_∞	τ (ns)	γ_μ	σ_{dc} (mS/m)
dry sand (ds)	5.7	3.4	8.0	0.70	1.14	1.02	15.0	1.0	0.45
moist sand	8.9	5.6	11.0	0.75	1.15	1.01	15.0	1.0	2.0
wet sand	29.0	25.6	22.2	0.88	1.17	1.00	15.0	1.0	6.06
clay (30% water)	43.0	20.7	18.3	0.66	1.10	1.00	25.0	1.0	42.5

materials.

In Turner and Siggins (1994) approximation, the slope of the attenuation curve is characterized with a constant Q^* parameter which gives the attenuation coefficient as

$$\alpha|_{\omega_1}^{\omega_2} \approx \alpha_0 + \frac{\sqrt{\mu_0 \epsilon'_{\omega_0}}}{2Q^*} (\omega - \omega_0) \quad (10)$$

where ω_0 is the reference frequency and α_0 is the value of α at ω_0 . By taking the first order Taylor expansion of Equation 8 about some center frequency, ω_0 , assuming that $\delta\epsilon'/\delta\omega \approx 0$, and utilizing the functional form for the complex dielectric permittivity given by Equation 9, I derive the following linear approximation to the attenuation coefficient

$$\alpha|_{\omega_1}^{\omega_2} \approx \alpha_{\omega_0} + \frac{1}{2} \sqrt{\frac{\mu_0}{\epsilon'_{\omega_0}}} \epsilon''_{\omega_0} \left(1 + \gamma - \frac{2\gamma(\omega_0\tau)^{2\gamma}}{1 + (\omega_0\tau)^{2\gamma}} \right) (\omega - \omega_0) \quad (11)$$

Combining Equations 10 and 11, I find Q^* in terms of the Cole-Cole parameters

$$\frac{1}{Q^*} = \frac{\epsilon''_{\omega_0}}{\epsilon'_{\omega_0}} \left[1 + \gamma - \frac{2\gamma(\omega_0\tau)^{2\gamma}}{1 + (\omega_0\tau)^{2\gamma}} \right] \quad (12)$$

When ω_0 is much higher than the relaxation frequency ($\omega_0\tau \gg 1$), Equation 12 reduces to

$$\frac{1}{Q^*} = \frac{\epsilon''_{\omega_0}}{\epsilon'_{\omega_0}} [1 - \gamma] \quad (13)$$

When ω_0 is much lower than the relaxation frequency ($\omega_0\tau \ll 1$) Equation 12 becomes

$$\frac{1}{Q^*} = \frac{\epsilon''_{\omega_0}}{\epsilon'_{\omega_0}} [1 + \gamma] \quad (14)$$

For Debye relaxation (Debye, 1945), $\gamma = 1$ and we see that Equations 13 and 14 give Q^* as a simple function of the ratio of real and imaginary parts of the complex dielectric permittivity, or the phase tangent. Often however, GPR operates near the relaxation frequency (Figure 1), which requires the more complicated form (Equation 12). Given Equations 12-14, it may be possible to estimate the Cole-Cole parameters from

GPR data by measuring Q^* with several different frequency antennas. In the following section I describe a method to measure Q^* .

Measuring Q^* from Reflection Data

An inherent non-uniqueness between reflectivity and the DC component of attenuation α_0 exists. Thus, measuring α_0 from surface GPR data is difficult without additional measurements such as complex resistivity. However, by measuring the shift in the signal spectrum through time using time-frequency analysis it is possible to isolate the frequency dependent component of attenuation given by the second term of Equation 11.

It is clear from Equation 8 that as the signal propagates, high frequencies are attenuated more strongly than low frequencies resulting in a spectral shift toward lower frequencies. We can use this spectral shift to measure Q^* from field data using the frequency shift method (Quan and Harris, 1997). The source waveform of some commercially available pulsed GPR systems approximates a Ricker wavelet. After propagating through a material for some time t , the signal spectrum is given by

$$S_t = \omega^2/\omega_0^2 \exp\left[1 - \omega^2/\omega_0^2\right] \exp\left[-\frac{\alpha(\omega)t}{\sqrt{\epsilon'\mu}}\right] \quad (15)$$

where ω_0 is the maximum amplitude of the source spectrum. Setting the derivative of Equation 15 equal to zero, and using Equation 10, the shift in peak frequency of the spectrum is related to Q^* by

$$\frac{1}{Q^*} = \frac{4(\omega_0^2 - \omega_t^2)}{t \omega_0^2 \omega_t} \quad (16)$$

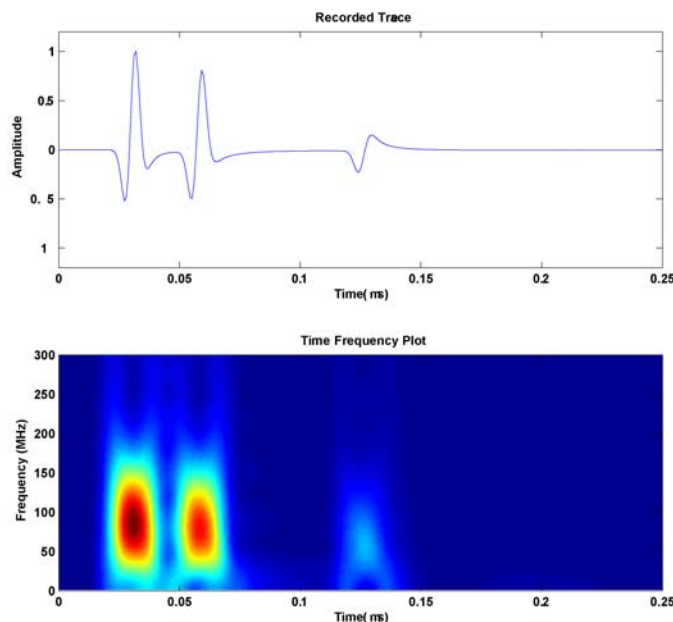


Figure 2: t-f distribution computed using the STFT for a synthetic signal with a 100 MHz source wavelet. In this model the peak frequency decays from 85 MHz to 56 MHz between the first and third reflections. See Figure 3 for model.

where ω_t is the spectral maxima at time t . Quan and Harris (1997) derive analogous expressions for centroid frequency shift for gaussian and boxcar spectra.

To extract Q^* from field data it is necessary to estimate the signal spectrum at horizons bounding the target interval. Estimating the source spectrum is not trivial in field data because it is a function of antenna coupling and near source dielectric properties. From Equation 16, the spectra of any event may be used as the reference spectrum to estimate the effective interval Q^* for any successive event.

It is also necessary to choose events for attenuation analysis. I normally pick significant horizons manually, then identify the local maxima of the envelope function within a time gate bounding the horizon. The reflection spectra is taken from the t-f distribution at the peak of the envelope function

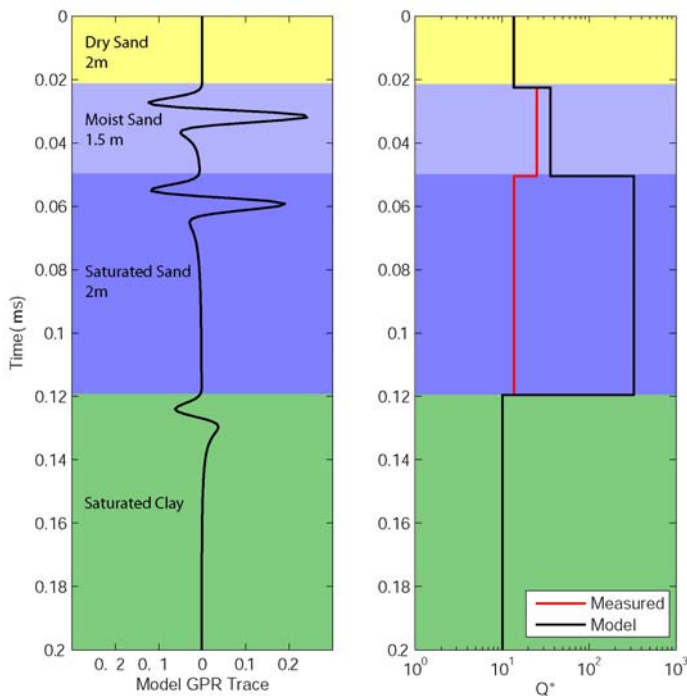


Figure 3: Model GPR data with the parameters listed in Table 1. There is significant divergence of the apparent Q^* value from the actual value, particularly in the saturated sand layer. This divergence is caused by spectral distortion due to frequency dependent reflection.

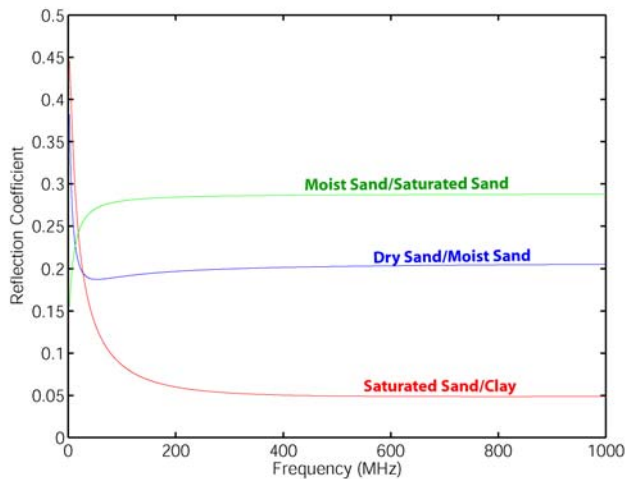


Figure 4: For the model shown in Figure 3, the reflection coefficients have a strong frequency dependence, particularly for the clay reflection. Spectral distortion due to frequency dependent reflectivity can mask the effect of intrinsic attenuation. (Plots are the absolute values)

for a given horizon. A number of methods are available to compute the t-f spectra of the data such as the short-time Fourier transform (STFT, Figure 2) or wavelet decompositions such as described by Bradford and Wu (1997). Alternatively, if the signal to noise ratio is high, the instantaneous frequency at the peak of the envelope function provides a reliable estimate of the average frequency of the reflection (Robertson and Nagomi, 1984). I analyzed all data presented here with the three methods noted above and found that the methods gave comparable results.

The Problem with the Q^ Measurement in Reflection Data: Defining the Dispersion Parameter*

One of the commonly recognized problems with Q^* analysis is that a number of factors can alter the source spectrum that are unrelated to the intrinsic attenuation. These include thinbed interference, multipathing, and scattering losses (Olhoeft and Capron, 1994). In addition to these factors, frequency dependent reflection coefficients can significantly alter the spectrum leading to bias in the Q^* estimate. As a test, I constructed a simple layered subsurface model representing an unconfined aquifer in sandy sediments with a clay aquitard at the base (Figure 3) using the Cole-Cole parameters given in Table 1. I then computed the response to the model for a 100 MHz source wavelet using a ray based modeling code that uses the complex wavenumber in a frequency domain computation to estimate wavelet distortion and traveltime along a given raypath (Bradford, 1999). Comparing the interval Q^* measured from the model data with Q^* computed from the attenuation coefficient curves (Figure 3) it is clear that the measured Q^* differs dramatically from the intrinsic Q^* value. This difference arises entirely from changes in the dispersion curve across layer boundaries leading to strong frequency dependence in the reflection coefficients (Figure 4). This effect is most obvious at the water-saturated sand/clay reflection. At this interface the reflection coefficient at low frequencies is larger than at high frequencies. This difference causes a spectral shift toward lower frequencies making the Q^* measured

from the data much lower than the modeled value.

Given this observation, I define the dispersion parameter, D , as

$$D = \frac{1}{Q^*} \quad (17)$$

Use of this nomenclature avoids the implication of a measurement of intrinsic attenuation that defines the Q^* parameter. D has high values when there is strong distortion of the spectrum. It is important to recognize that thin beds or frequency dependent reflection can cause the spectrum to shift toward higher frequencies. In this case, the dispersion parameter is negative.

Clearly the subsurface characteristics that lead to the measured D value are complicated and in general, it may not be possible to isolate a particular contribution to the observed spectral changes. While it may not be possible to differentiate changes in dispersion due to intrinsic attenuation from dispersion due to frequency dependent reflection or other effects, we can use the measurement to look for spectral anomalies in the subsurface that are related to target materials. Below, I demonstrate that qualitative analysis of the D parameter can be a strong indicator of lateral changes in dispersion characteristics related to the presence of contaminants.

Field Studies

Detection of NAPL Contaminants

Of many potential uses for GPR attenuation analysis, detection of non-polar organic liquid contaminants may prove a particularly valuable application. These contaminants are collectively referred to as non-aqueous phase liquids (NAPL) due to their low solubility in water. NAPLs are subcategorized by their density relative to water; dense NAPLs (DNAPL) are denser than water and light NAPLs (LNAPL) are lighter than water. DNAPLs tend to sink through the water column until they reach a low permeability layer, whereas LNAPLs tend to remain near the water table with free product floating on the water column and residual LNAPL present in a smear zone above and below the water table. Both LNAPLs and DNAPLs leave a zone of residual contamination along their migration routes. Chlorinated solvents (DNAPL) and fuel hydrocarbons (LNAPL) are common examples.

NAPLs typically have low relative permittivity ($\epsilon/\epsilon_0 \sim 2.5$) and low electric conductivity ($\sigma \sim 0.01 - 0.1$ mS/m) relative to fresh water ($\epsilon/\epsilon_0 \sim 81$, $\sigma > 1$ mS/m) which make them attractive targets for characterization using electrical geophysical methods. Of particular importance for this study, NAPLs are electrically non-dispersive. When NAPL displaces water in the sediment pore space, a zone of anomalous electrical properties may occur. A first order conceptual model is based on the premise that NAPL contaminated zones will have low permittivity and low conductivity relative to the surrounding formation. A number of controlled spill experiments are consistent with this model (Bradford, 2004; Brewster and Annan, 1994; Campbell et al., 1995; DeRyck et al., 1993). This model has also proved effective in the interpretation of geophysical data acquired over a fresh LNAPL spill (Orlando, 2002) and over aged LNAPL and DNAPL spills at another field site (Bradford and Deeds, in press; Lien and Enfield, 1998; Newmark et al., 1998). However, aged LNAPL spills at some sites have anomalously high electric conductivity (Atekwana et al., 2000; Monier-Williams, 1995; Sauck et al., 1998). This discrepancy stems from the incorrect assumption that the electric properties of the unaltered LNAPL control the electric properties of the contaminated zone (Sauck, 1998). In either case, frequency-dependent GPR attenuation analysis only

requires that an anomaly in the dispersion characteristics of the material is present. Below, I discuss detection of contaminant induced dispersion anomalies at two NAPL contaminated sites.

Cape Fear Wood Preserving Site (Creosote)

The Cape Fear Wood Preserving Site, Fayetteville, North Carolina, produced creosote-treated wood between 1953 and 1978. In 1977 the site was found to be contaminated with coal tar and coal tar creosote of which the primary constituents are PAHs (DNAPL). In the mid 1980s remediation activities were initiated including excavation and removal of some contaminated soils. In 2001 and 2002 additional characterization revealed that significant quantities of residual and free phase DNAPL remained. Current mitigation activities include a new round of characterization and remediation design. Shallow sediments at the site consist of fine grained sands and silty sands to a depth of about 10 m where a thick silty clay unit is present. A shallow (1 m) water table is present in the unconfined surficial aquifer. (Black and Veach Special Projects Corp., 2002)

The primary objectives of the radar study at the Cape Fear Site were 1) to map the shallow stratigraphy, and 2) testing methods for direct detection of DNAPL. Initial tests indicated that the site was suitable for radar investigation with good data quality to depths of 6 - 11 m.

Line 2 is typical of data acquired elsewhere at the site (Figure 5). The profile was located to span an area of zero or low contamination to a zone of high contamination. To broaden the signal spectrum, I

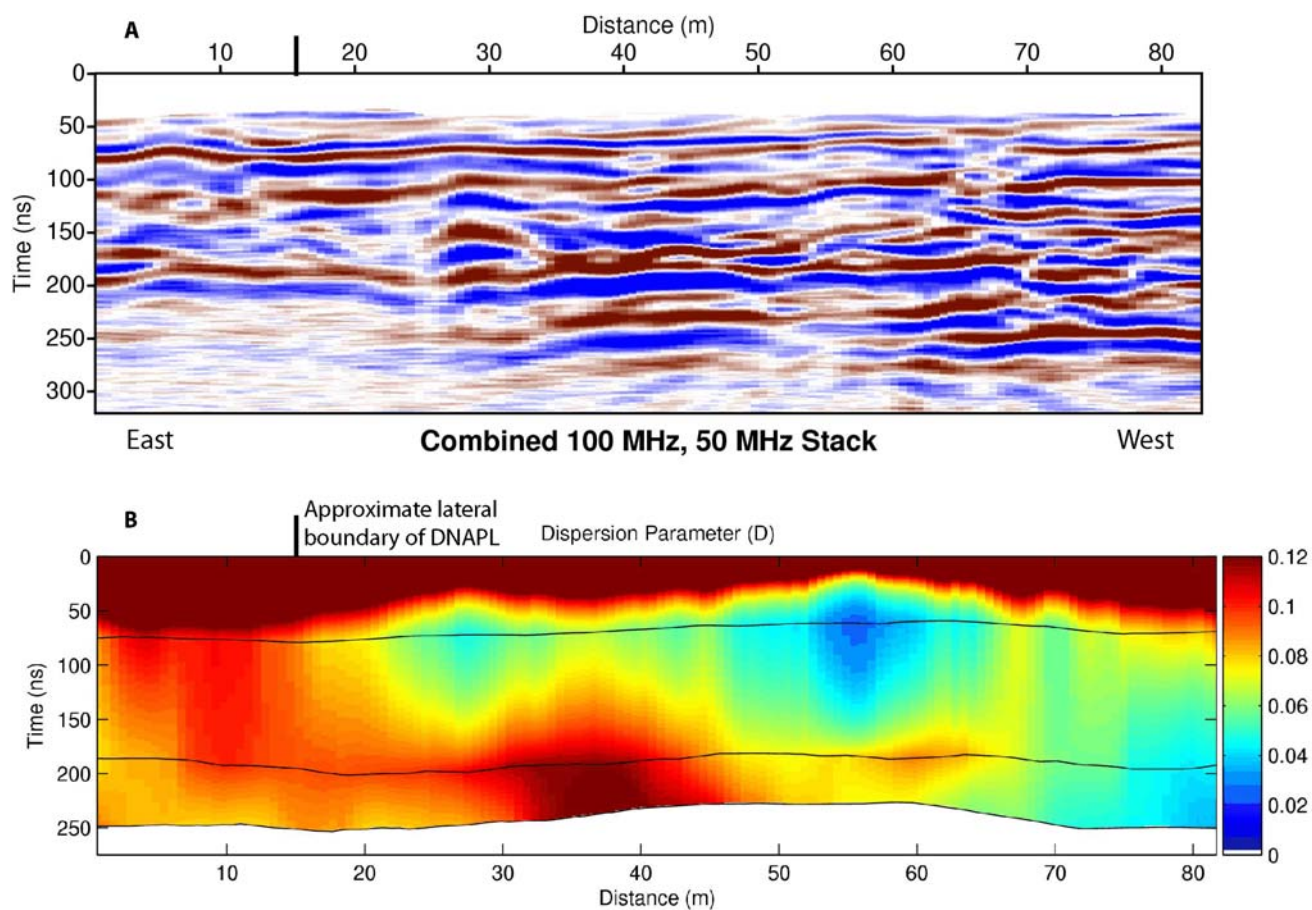


Figure 5: A) Combined 50 and 100 MHz 25-fold stack. The soil disturbance due to excavation and backfill is evident from 70 - 82 m. B) The D distribution at the Cape Fear site shows a zone of low dispersion that increases in thickness toward the west. The spatial distribution of decreased dispersion is consistent with significant creosote accumulations mapped using CPT LIF and ROST logs.

acquired coincident 50 MHz and 100 MHz profiles using a Sensors and Software PE 100A system. The data were acquired in continuous CMP mode with 25-fold common source gathers, 0.6 m source spacing, and 0.3 m receiver spacing. Prior to attenuation analysis, the processing stream consisted of a time zero drift correction, highpass dewow filter, a t^2 gain correction, stacking velocity analysis, NMO correction and stacking. Strong, laterally coherent reflections were recorded at depths up to 11 m (~250 ns) (Figure 5). For the attenuation analysis, I picked three horizons bounding two depth intervals; 3-7 m (70 - 190 ns) and 7-9 m (190 - 250 ns). These two intervals are bounded by laterally coherent, relatively high amplitude reflections and thus represent significant stratigraphic units. Note that from 70 - 82 m along Line 2, the interval from the surface to a depth of 6 m was previously excavated and backfilled, and therefore is not representative of the natural stratigraphy.

I computed the time-frequency transform using the STFT, then measured the maximum frequency in the spectrum for the three horizons. D was computed trace by trace relative to a laterally variable estimated source reference frequency. The reference frequency was scaled from the spectral peak along the shallowest horizon and had a mean of 68 MHz. Since I used a common reference spectrum for each reflection, D is a measure of the cumulative spectral distortion from the surface to each horizon. The dispersion image was computed by linear interpolation of D along the vertical axis.

There is a significant lateral decrease in the D distribution that thickens toward the west. This zone correlates well with the spatial distribution of DNAPL measured using CPT mounted laser induced fluorescence probes and direct borehole samples (Black and Veach Special Projects Corp., 2002). I conclude that the presence of DNAPL in the subsurface at this site produces a significant decrease in the dispersive properties of the bulk materials and that GPR is sensitive to this change.

Former Wurtsmith AFB NETTS

This site is a former fire training facility, designated FT-02, located on the now decommissioned Wurtsmith Air Force Base, Oscoda, Michigan. Over a period of about 24 years, large quantities of fuel were burned on open ground during weekly training exercises. A significant volume of hydrocarbons did not burn and seeped into the underlying aquifer. In 1982 a concrete catch basin was constructed to minimize the amount of contaminant reaching the subsurface. By the early 1990s, the free product plume was up to 0.3 m thick, and extended more than 180 m downgradient from FT-02 (Bermejo et al., 1997; Sauck et al., 1998).

The stratigraphy below the site consists of fine to medium grained sand and gravel deposits extending to a depth of approximately 20 m. Below this is a 6 - 30 m thick silty clay layer which is thought to be the lower boundary for contaminant migration. The surficial aquifer is unconfined, with the water table present 3 - 5 m below the surface. The site was formerly a National Environmental Technology Test Site (NETTS) and was the site of a long term natural bioremediation investigation. Although no longer an active NETTS site, the wealth of characterization data available make this an excellent location for a semi-controlled GPR field experiment. Central to the selection of this site for the current study are a series of geophysical investigations carried out by Sauck et al. (1998) and Bermejo et al. (1997). They found that the site provided excellent conditions for GPR with strong reflections well below the water table. Additionally, they found that there was a well defined, high attenuation anomaly coincident with the LNAPL plume. Through resistivity and self potential measurements, and by inference from the GPR data, they concluded that high electric conductivity was associated with both the LNAPL and the dissolved phase plume. This site provided an excellent opportunity to study a conductive type plume.

During July, 2002, we acquired 1676 linear m of multi-offset data, including a 930 m² 3D survey using both TE and TM modes. The 3D survey was oriented such that one edge of the plume would cross diagonally through the 3D patch. Additionally, data were acquired along two 122 m east/west profiles that bounded the 3D patch to the north and south. These profiles extended well beyond the east and west

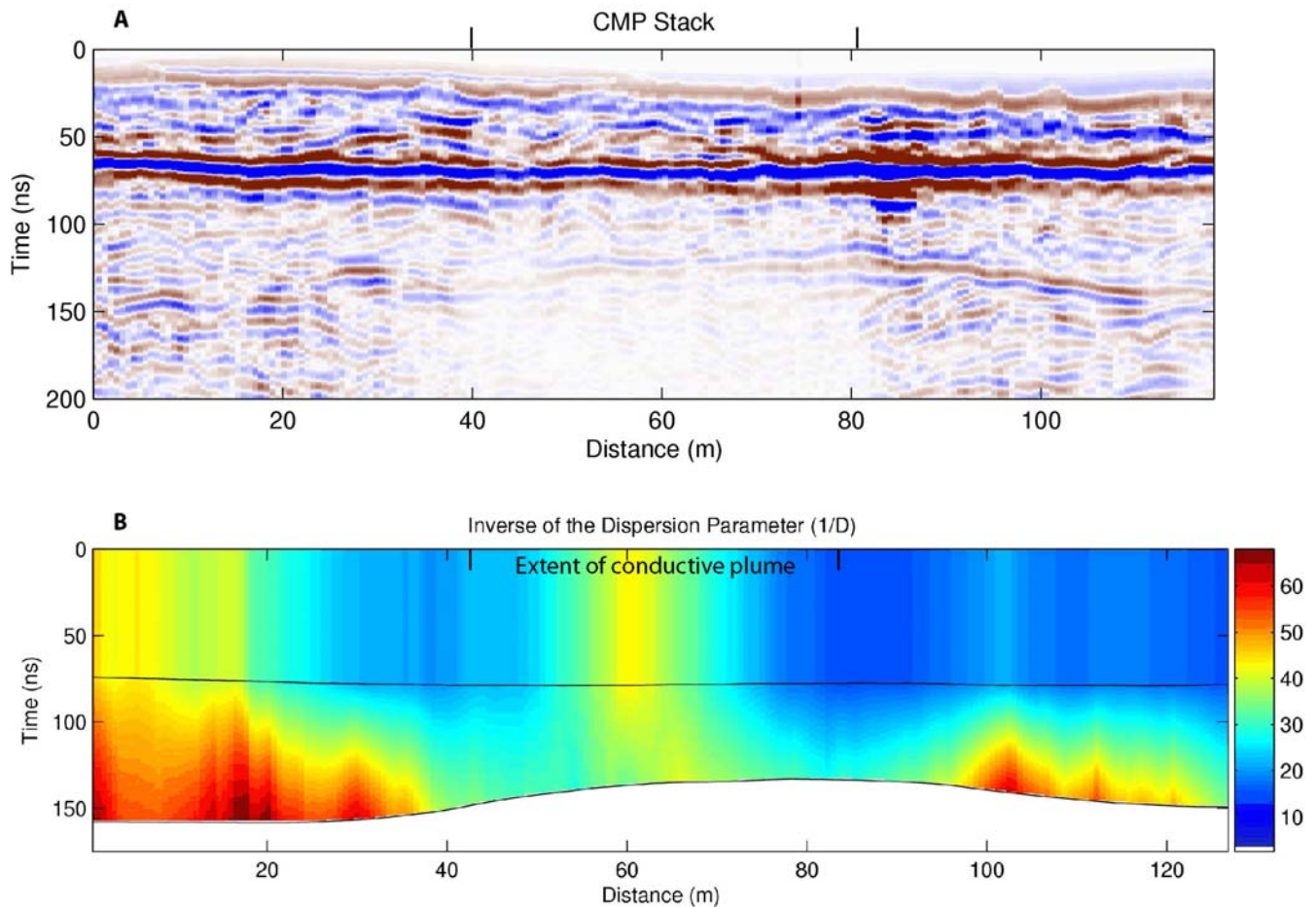


Figure 6: A) 25-fold stack of 100 MHz data acquired at the former Wurtsmith AFB. The water table reflection is at ~65 ns. B) Image of the inverse of the dispersion parameter, $1/D$. By plotting $1/D$ it is easier to visualize the zone of high dispersion below the water table from 40 - 90 m. At this site, increased dispersion correlates with increased DC conductivity that is caused by increase in the dissolved solid concentration resulting from biodegradation of the hydrocarbon plume (Sauck et al., 1998).

boundaries of the plume. Here I discuss the results along one of the 122 m profiles. The data were acquired with 100 MHz antennas in continuous CMP mode with 25-fold common source gathers, 0.6 m source interval, and a 0.3 m receiver interval. The processing stream for attenuation analysis was the same as that described for the Cape Fear site in the previous section, with the exception that I used a constant reference frequency of 90 MHz.

My first objective was to reproduce the results of Sauck et al. (1998) and I found a similar attenuation anomaly. The zone of increased conductivity is most evident as an area of low reflection amplitudes, or “shadow zone”, beginning just below the water table and extending the full length of the record (Figure 6). For the attenuation analysis, I picked two horizons: the water table reflection at ~ 65 ns (~ 4m) and a horizon that varied from 120 ns to 150 ns (2 - 3 m below the water table) within the water saturated zone. The deeper horizon is laterally discontinuous from a lateral position of 0 - 25 m, then continuous across the rest of the profile. The measured D distribution shows a distinct zone of increased dispersion that correlates with the zone of increased electric conductivity (Figure 6). I conclude that the increase in electric conductivity, which is a secondary effect caused by biodegradation of the hydrocarbons, alters the dispersion characteristics of the bulk formation and masks any decrease in dispersion due to the

residual LNAPL that remains in the system. Of additional interest at this site is that the D value is generally higher in the vadose zone than in the saturated zone. This observation could be indicative of increased dispersion in the unsaturated sediments as in the synthetic model presented earlier (Figures 1 - 4) or could simply be caused by a decrease in the frequency content of the water table reflection due to a diffuse boundary at the capillary fringe.

Conclusions

Linearizing the imaginary component of the wavenumber in frequency using the low loss approximation provides a formulation relating the Q^* parameter to the Cole-Cole parameters. Measuring Q^* over a range of GPR frequencies may provide a method for estimating Cole-Cole parameters. However, frequency dependent reflection, interference, and thinbed tuning alter the frequency spectrum of a reflected signal making direct measurement of Q^* difficult. For this reason I define the dispersion parameter D , whose measurement is mathematically equivalent to Q^* , but the new parameter definition recognizes that the intrinsic attenuation is only one contributor to the spectral shift observed in GPR data. The dispersion parameter is then a measure of the frequency dependence of the complex dielectric permittivity at high frequencies. Although potentially correlated, D provides fundamentally different information than low frequency EM measurements. It is important to recognize that geometric effects unrelated to intrinsic material properties contribute to D in reflection data and in some cases may be the predominant mode of spectral distortion. At two field sites, I have shown that D is a qualitative indicator of electric property anomalies caused by the presence of organic contaminants. At the Cape Fear Wood Preserving site, the presence of DNAPL produced a zone of low dispersion, while at the former Wurtsmith AFB increased conductivity caused by biodegradation of LNAPL contamination produced a zone of relatively high dispersion. These field results are promising and the methodology may prove valuable for quantitative subsurface characterization using GPR, but additional field studies are necessary to investigate the full potential.

References

- Atekwana, E.A., Sauck, W.A., and Werkema Jr., D.D., 2000, Investigations of geoelectrical signatures at a hydrocarbon contaminated site: *Journal of Applied Geophysics*, v. 44, p. 167-180.
- Bermejo, J.L., Sauck, W.A., and Atekwana, E.A., 1997, Geophysical discovery of a new LNAPL plume at the former Wurtsmith AFB, Oscoda, Michigan: *Groundwater Monitoring and Remediation*, v. 17, p. 131-137.
- Black and Veach Special Projects Corp., 2002, Final NAPL Investigation Report: Cape Fear Wood Preserving Site Fayetteville, Cumberland County, North Carolina: Alpharetta, GA, U.S. Environmental Protection Agency.
- Bradford, J.H., 1999, Characterizing shallow aquifers with wave-propagation based geophysical techniques: Imaging and attribute analysis [Ph. D. thesis]: Houston, Rice University.
- , 2004, 3D Multi-offset, multi-polarization acquisition and processing of gpr data: a controlled DNAPL spill experiment, SAGEEP 2004 Symposium on the Application of Geophysics to Environmental and Engineering Problems: Colorado Springs, CO, Environmental and Engineering Geophysical Society, p. 514-527.
- Bradford, J.H., and Deeds, J.C., in press, Ground-penetrating radar theory and application of thinbed offset dependent reflectivity: *Geophysics*.
- Bradford, J.H., and Wu, Y., 1997, Time-frequency representation of seismic signals via matching pursuit decomposition with complex Ricker wavelets, AGU Fall meeting, Volume 78: EOS Supplement:

- San Francisco, American Geophysical Union, p. 33.
- Brewster, M.L., and Annan, A.P., 1994, Ground-penetrating radar monitoring of a controlled DNAPL release: 200 MHz radar: *Geophysics*, v. 59, p. 1211-1221.
- Cai, J., and McMechan, G.A., 1999, 2-D ray-based tomography for velocity, layer shape, and attenuation from GPR data: *Geophysics*, v. 64, p. 1579-1593.
- Campbell, D.L., Lucious, J.E., Ellefson, K.J., and Deszcz-Pan, M., 1995, Monitoring of a controlled LNAPL spill using ground-penetrating radar, SAGEEP '95: Symposium on the Application of Geophysics to Environmental and Engineering Problems: Proceedings: Keystone, CO, Environmental and Engineering Geophysical Society, p. 511-517.
- Chakraborty, A., and Okaya, D., 1995, Frequency-time decomposition of seismic data using wavelet-based methods: *Geophysics*, v. 60, p. 1906-1916.
- Chang, P.Y., Alumbaugh, D., Brainard, J., and Hall, L., 2002, Using cross borehole ground penetrating radar attenuation tomography for characterizing soil properties in the vadose zone during a two-stage infiltration test, 72th Ann. Internat. Mtg., Soc. Expl. Geophys.: Expanded abstracts, Society of Exploration Geophysicists, p. 1563-1566.
- Cole, K.S., and Cole, R.S., 1941, Dispersion and absorption in dielectrics, I, alternating current characteristics: *J. Chem. Phys.*, v. 9, p. 341-351.
- Day-Lewis, F.D., Harris, J.M., and Gorelick, S.M., 2002, Time-lapse inversion of crosswell radar data: *Geophysics*, v. 67, p. 1740-1752.
- Day-Lewis, F.D., Lane, J.W., Harris, J.M., and Gorelick, S.M., 2003, Time-lapse imaging of saline-tracer transport in fractured rock using difference-attenuation radar tomography: *Water Resources Research*, v. 39, p. 1290, doi:10.1029/2002WR001722.
- Debye, P.J., 1945, *Polar Molecules*, Dover Publ. Inc.
- DeRyck, S.M., Redman, J.D., and Annan, A.P., 1993, Geophysical monitoring of a controlled kerosene spill, SAGEEP '93 Symposium on the Application of Geophysics to Environmental and Engineering Problems: Proceedings, Environmental and Engineering Geophysical Society, p. 5-19.
- Goldstein, S.E., Johnson, T.C., Knoll, M.D., Barrash, W., and Clement, W.P., 2003, Borehole radar attenuation-difference tomography during the tracer/timelapse test at the Boise Hydrogeophysical Research Site, SAGEEP 2003 Symposium on the Application of Geophysics to Environmental and Engineering Problems: San Antonio, TX, Soc. Eng. Env. Geophys., p. 147-162.
- Grandjean, G., Gourry, J.C., and Bitri, A., 2000, Evaluation of GPR techniques for civil-engineering applications; study on a test site: *Journal of Applied Geophysics*, v. 45, p. 141-156.
- Griffiths, D.J., 1989, *Introduction to electrodynamics*: Englewood Cliffs, NJ, Prentice-Hall, 532 p.
- Irving, J.D., and Knight, R.J., 2003, Removal of wavelet dispersion from ground-penetrating radar data: *Geophysics*, v. 68, p. 960-970.
- Lane, J.W., Day-Lewis, F.D., Harris, J.M., Haeni, F.P., and Gorelick, S.M., 2000, Attenuation-difference radar tomography: Results of a multiple-plane experiment at the U.S. Geological Survey fractured-rock research site, Mirror Lake, New Hampshire, *in* Noon, D.A., Stickley, G.F., and Longstaff, D., eds., *GPR 2000, Eighth International Conference on Ground Penetrating Radar, Volume 4084: Proceedings, International Society for Optical Engineering*, p. 666-675.
- Li, X., and Ulrych, T.J., 1996, Multi-scale attribute analysis and trace decomposition, 66th Ann. Internat. Mtg.: Expanded abstracts, Soc. Expl. Geophys., p. 1634-1637.
- Lien, B.K., and Enfield, C.G., 1998, Delineation of subsurface hydrocarbon contaminant distribution using a direct push resistivity method: *Journal of Environmental and Engineering Geophysics*, v. 2, p. 173-179.
- Liu, L., Lane, J.W., and Quan, Y., 1998, Radar attenuation tomography using the centroid frequency downshift method: *Journal of Applied Geophysics*, v. 40, p. 106-116.

- Liu, L., and Quan, Y., 1997, GPR attenuation tomography for detecting DNAPLs, SAGEEP '97 Symposium on the Application of Geophysics to Environmental and Engineering Problems: Reno, Nevada, Environmental and Engineering Geophysical Society, p. 241-243.
- Monier-Williams, M., 1995, Properties of light non-aqueous phase liquids and detection using commonly applied shallow sensing geophysical techniques, SAGEEP '95 Symposium on the Application of Geophysics to Environmental and Engineering Problems: Proceedings: Keystone, CO, Environmental and Engineering Geophysical Society, p. 1-15.
- Morlet, J., Arens, G., Fourgeau, E., and Giardi, D., 1982a, Wave propagation and sampling theory - Part I: Complex signal scattering in multilayered media: *Geophysics*, v. 47, p. 203-221.
- , 1982b, Wave propagation and sampling theory - Part II: Sampling theory and complex waves: *Geophysics*, v. 47, p. 222-236.
- Newmark, R.L., Daily, W.D., Kyle, K.R., and Ramirez, A.L., 1998, Monitoring DNAPL pumping using integrated geophysical techniques: *Journal of Environmental and Engineering Geophysics*, v. 3, p. 7-13.
- Olhoeft, G.R., and Capron, D.E., 1994, Petrophysical causes of electromagnetic dispersion, 5th Internat. Conf. GPR: Proceedings: Kitchener, Ontario, Canada, Waterloo Center for Groundwater Research, p. 145-152.
- Olhoeft, G.R., and Strangway, D.W., 1974, Magnetic relaxation and the electromagnetic response parameter: *Geophysics*, v. 39, p. 302-311.
- Orlando, L., 2002, Detection and analysis of LNAPL using the instantaneous amplitude and frequency of ground-penetrating radar data: *Geophysical Prospecting*, v. 50, p. 27-41.
- Peterson, J.E.J., 2001, Pre-inversion corrections and analysis of radar tomographic data: *J. of Env. Eng. Geophys.*, v. 6, p. 1-18.
- Quan, Y., and Harris, J.M., 1997, Seismic attenuation tomography using the frequency shift method: *Geophysics*, v. 62, p. 895-905.
- Robertson, J.D., and Nagomi, H.H., 1984, Complex seismic trace analysis of thin beds: *Geophysics*, v. 49, p. 344-352.
- Sauck, W.A., 1998, A conceptual model for the geoelectrical response of LNAPL plumes in granular sediments, SAGEEP '98 Symposium on the Application of Geophysics to Environmental and Engineering Problems: Proceedings: Chicago, IL, Environmental and Engineering Geophysical Society, p. 805-817.
- Sauck, W.A., Atekwana, E.A., and Nash, M.S., 1998, High conductivities associated with an LNAPL plume imaged by integrated geophysical techniques: *Journal of Environmental and Engineering Geophysics*, v. 2, p. 203-212.
- Tobbock, T., Steeghs, P., Drijkoningen, G.G., and Fokkema, J.T., 1996, Decomposition of seismic signals via time-frequency representations, 66th Ann. Internat. Mtg.: Expanded abstracts, Soc. Expl. Geophys., p. 1638-1641.
- Turner, G., 1994, Subsurface radar propagation deconvolution: *Geophysics*, v. 59, p. 215-223.
- Turner, G., and Siggins, A.F., 1994, Constant Q attenuation of subsurface radar pulses: *Geophysics*, v. 59, p. 1192-1200.
- Zhou, C., and Liu, L., 2001, Nonlinear inversion of borehole-radar tomography data to reconstruct velocity and attenuation distribution in Earth materials: *Journal of Applied Geophysics*, v. 47, p. 299-308.